



Article

# Long-Exposure Air and Steam Oxidation Characteristics of IN 617 Alloys

Rishikesh Karthikeyan <sup>1</sup>, Satyanaryanan Seshadri <sup>1,\*</sup> , V Subramanya Sarma <sup>2</sup> and M Kamaraj <sup>2</sup>

<sup>1</sup> Department of Applied Mechanics, IIT Madras, Chennai 600036, India

<sup>2</sup> Department of Materials and Metallurgical Engineering, IIT Madras, Chennai 600036, India

\* Correspondence: satya@iitm.ac.in

**Abstract:** India's growing power demands and emission norms require more efficient coal-based power plants. The shifting of power plants from subcritical to ultra-supercritical (USC) steam conditions could improve efficiency by 12% and reduce CO<sub>2</sub> emissions by 35%. There is a need to develop and qualify materials under ultra-supercritical steam conditions with high temperatures and high pressures in laboratory scale. The sample materials were exposed to high temperatures of 700 °C under air and high pressure steam at 700 °C/243 bars for 1000 h in as-received and grain-boundary-enhanced conditions. Grain boundary enhancement included optimization of a thermo-mechanical process involving cold rolling and annealing of samples. The effect of air and steam oxidation on IN 617, a nickel-based candidate superalloy, was analysed. Steam oxidation was performed on a custom-built PARR 4650 series autoclave, and the oxidized samples were characterised under scanning electron microscopy, to evaluate the oxide scales. The grain-boundary-engineered material performed better than the as-received samples. IN 617 overall fared better under both air and steam conditions, with far less weight gains.

**Keywords:** ultra-supercritical; IN 617; grain boundary enhancement; grain size; oxide layer; weight gain; depletion layer; mechanism



**Citation:** Karthikeyan, R.; Seshadri, S.; Sarma, V.S.; Kamaraj, M. Long-Exposure Air and Steam Oxidation Characteristics of IN 617 Alloys. *Corros. Mater. Degrad.* **2023**, *4*, 90–103. <https://doi.org/10.3390/cmd4010006>

Academic Editor: Daniel John Blackwood

Received: 28 September 2022

Revised: 13 January 2023

Accepted: 17 January 2023

Published: 31 January 2023



**Copyright:** © 2023 by the authors. Licensee MDPI, Basel, Switzerland. This article is an open access article distributed under the terms and conditions of the Creative Commons Attribution (CC BY) license (<https://creativecommons.org/licenses/by/4.0/>).

## 1. Introduction

International Energy Agency statistics for world historical and projected global energy consumption, between 2009 and 2035, show that energy demand is increasing by 1.6% per annum [1]. The majority (about 40%) of the world's electricity is generated by coal-based power plants [2]. India's growing power demands and stringent emission norms require more efficient coal-based power plants. Most of India's power demands are met through coal-based power, due to the ready availability of cheap coal as fuel, an existing infrastructure and skilled manpower, all of which have rendered the country reliant on this technology. An average Indian power plant has an efficiency of 38% [3], which indicates that a large amount of coal needs to be burnt to produce valuable power. Emissions from power plants like SO<sub>x</sub> and NO<sub>x</sub> need to be kept within the standard limit of 100 mg/Nm<sup>3</sup>, as per pollution norms. India has decided to reduce its emissions to net zero by 2070 [4]: in order to meet this ambitious deadline, the country is slowly moving on to cleaner coal technology. To meet the energy demands, and to minimize the CO<sub>2</sub> emissions, the approach taken can either be to move on to non-conventional energy resources, or to run the existing plants more efficiently and cleanly. Already most of the country's inefficient subcritical plants are being phased out. The shifting of subcritical to ultra-supercritical steam conditions could improve efficiency by 12%, and reduce CO<sub>2</sub> emissions by 35%. The efficiency of power plants is a function of steam temperatures and pressures [5]; however, the transition to ultra-supercritical technology is strongly linked to the development of suitable materials that will withstand high temperatures and pressures. Oxidation and creep are major degradation mechanisms that the materials should be able to withstand at operating temperatures.

To study oxidation behaviour in a steam environment under high pressure, there is a need to develop and qualify materials under ultra-supercritical steam conditions at high temperatures and under high pressures of up to 710 °C and 350 bar [6]. The major bottleneck is the availability of advanced materials at a reasonable cost. The material selected should be reliable, and not susceptible to failure at high temperatures and under the pressure conditions of steam. In India, a consortium has been formed by the Indira Gandhi Centre for Atomic Research (IGCAR), Bharat Heavy Electricals Limited (BHEL) and the National Thermal Power Corporation Limited (NTPC), to build India's first advanced ultra-supercritical power plant: they have selected Ni-base superalloy IN 617 and austenitic stainless steel 304HCu as candidate materials for superheater and reheater tubes, respectively. There is a limited amount of data available on how these materials perform in a high-pressure steam environment that simulates real-life power plant conditions. There is a need to perform these tests under lab conditions, to generate data for steam oxidation studies of the long exposures of 304HCu and IN 617.

Archana et al. (2021) studied the oxidation characteristics of IN 617 under high-temperature air and steam at 750 °C for 500 h. The oxide formed was multifaceted. Weight gain and oxide scale thickness grew with exposure time. Denser oxide scales, which were formed under steam and oxide layers, were composed of chromium oxide. The scales were crack-free, without spallation [7]. The water was sent in, inside a tubular furnace maintained at test temperature. High-pressure conditions, such as 250 bar, were not maintained.

Hari et al. (2020) studied the oxidation of alloy 617 of optimised chemical composition under air at 700 °C for up to 5000 h, at intervals of 500 h each: metallic agglomerates were observed after 4000 h; no weight change was observed at the end of the exposure. The oxides were entirely made of chromium oxide. The scale thickness increased with exposure time. Titanium and aluminium underwent internal oxidation, and those sites resulted in increased permeability of the outward cations [8].

Satszewska and Scendo et al. (2016) analysed the mechanism and oxidation kinetics of IN 617 and IN 625. An air oxidation experiment was performed non-isothermally at 100–1200 °C for exposures up to 96 h. The external oxides consisted of Cr<sub>2</sub>O<sub>3</sub>, and the internal layer consisted of NiCr<sub>2</sub>O<sub>4</sub>. The alloy 625 consisted of Nb<sub>2</sub>O<sub>5</sub>, and the alloy 617 consisted of MoO<sub>2</sub> and CoO in addition to the chromium-based scales. Both alloys followed the parabolic rate law for oxide growth [9].

Holcomb et al. (2014) conducted high-temperature steam oxidation of alloys for advanced ultra-supercritical conditions at 267 ± 17 bar/670 °C, and compared the results to 670 °C/1 bar for 293 h. Alloy TP304H had a thin scale of 0.4 µm under 1 bar, while it had a scale of 15 µm under 267 bar. The outer layer consisted of porous Fe-oxide, while the inner layer was a dense layer of Fe-Cr spinel. Coarse grain oxidised much faster than fine grain. At higher pressures, fine grain behaved like coarse grain; therefore, no compact chromia scales were found at higher pressures. The critical chromium content required for forming protective chromia scales increased with the increase in pressure. The nickel-based alloy had a thin, compact and dense chromia scale at 1 bar, while at 267 bar the chromia scales were thick. The increase in hydrogen injected into the metal increased the solid state diffusion [10]. In our case, we needed to have reliable data on the steam oxidation behaviour of the candidate material for a longer duration.

Yang et al. (2020) analysed the high temperature oxidation of alloys under supercritical water at 650 °C for 320 h. IN 617 and IN 740 formed bar-like oxides. HR6W formed two oxides: one of large (2–3 µm) discontinuities, and randomly spread, while the other was little (<1 µm). HR6W oxides spalled at different stage of oxidation, and had higher oxidation. Nickel-based alloy detected higher chromium than nickel, due to chromium oxides. The oxide scale thickness in HR6W was thrice that of the nickel alloys. The oxide film structure was similar overall (Cr-rich layer and Fe-rich layer) [11].

There is a dearth of research on high-pressure steam environments that can simulate real-life power plant conditions: there is a need to perform these tests under lab conditions, before scaling up. A sufficient amount of data needs to be generated from studies of IN

617 steam oxidation under long exposures, before a decision can be taken about the use of IN 617 in power plants. IIT Madras has established an ultra-supercritical steam test facility to test materials, coatings and weldments under high-temperature and high-pressure conditions of 750 °C/150 bar, 700 °C/241.1 bar and 650 °C/360 bar for continuous long exposures of 1000 h. In this paper, the effect of steam oxidation on IN 617 was characterised after studies of 1000 h exposure to air at 700 °C and to steam at 700 °C/243 bar. The oxide scales were analysed and confirmed under scanning electron microscopy (SEM) and X-ray diffraction (XRD), for morphological and compositional data.

## 2. Materials and Testing Procedure

### 2.1. Initial Condition

A nickel-based superalloy, IN 617, was obtained from VDM Metals GmbH, Germany, solution-annealed at 1175 °C, then quenched in water. The starting microstructure of the IN 617 was abbreviated to an as-received AR sample. The AR sample was subjected to cold rolling at 5%, 10% and 15%, followed by annealing at 1000, 1050 and 1100 °C for durations of 0.5, 1 and 2 h, and was subsequently quenched in water. The optimized parameters that led to the grain boundary engineering (GBE) microstructure were achieved at 15% cold-rolled and subsequent annealing at 1100 °C for 1 h, followed by water quenching of the IN 617 alloy. Then, the GBE samples were abbreviated to IN 617 GBE [12]. The composition obtained from the manufacturer is tabulated in Table 1, and was re-verified in IIT Madras. The hardness and tensile strength of the tested specimen were found to be 197 HV and 812 MPa, respectively. The initial SEM image and the XRD pattern results are shown in Figure 1, obtained by Thermofischer Apreo 2S. The initial microstructure included titanium precipitates along with the matrix phase elements. The precipitates are seen as white spots. No solution annealing treatment was performed on the as-received sample. The coupons were taken in the form of 10 mm × 10 mm square plates of 2.5 mm thickness for the air oxidation experiment. For steam oxidation, the same coupons had a 3 mm drill made, using a solid carbide tool. All the coupons were uniformly polished to 1200 grit, using silicon carbide abrasive paper. The initial X-ray diffraction pattern of the as-received sample consisted of Nickel-base peaks, while secondary phase peaks were not found predominantly. The precipitates were mostly Ti(C,N). The initial XRD analysis was done, so that it could be compared to the XRD data that was obtained at the end of oxidation for the same material. The XRD result was in line with the literature data [13]. The flowchart in Figure 2. explains the experimental method followed.

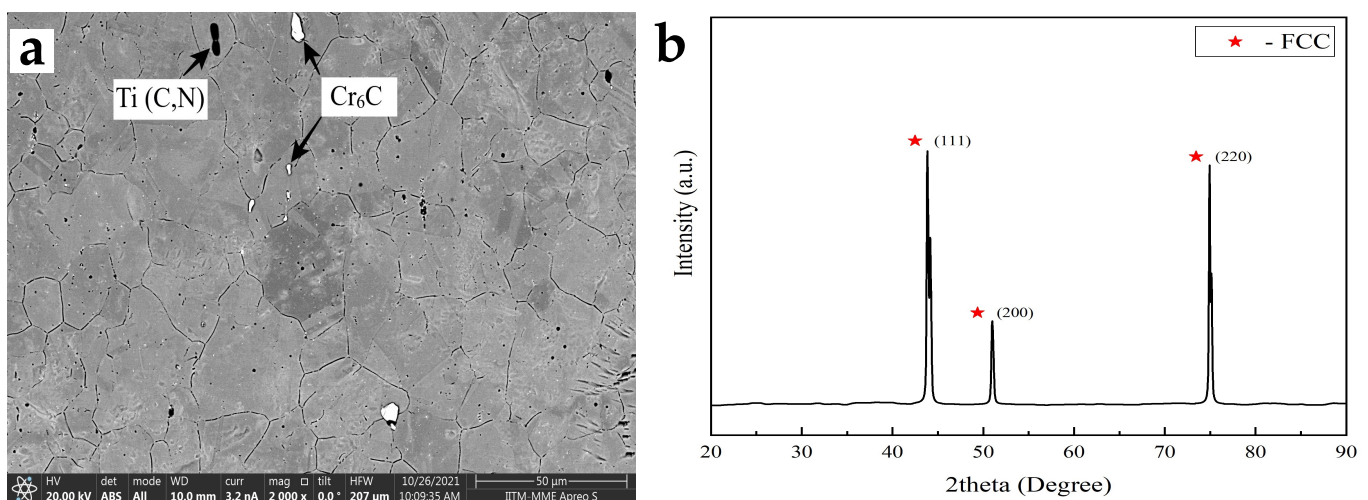
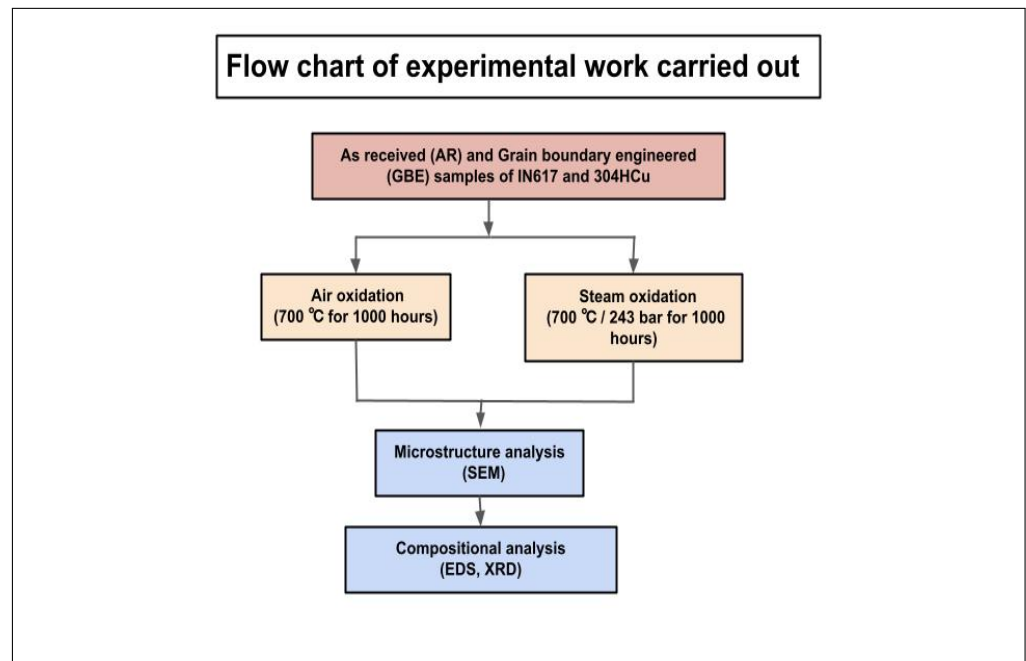


Figure 1. (a) Initial SEM micrograph and (b) XRD pattern of sample IN 617.

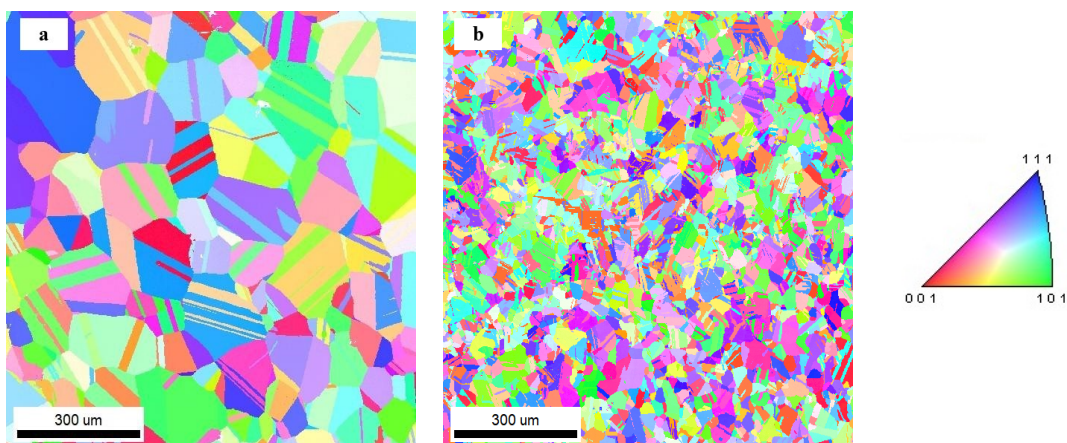
**Table 1.** Material composition of IN 617.

ELEMENTS	Ni	Cr	Co	Mo	Fe	Ti	Al	Mn	Si	Cu
wt. %	53.46	22.45	11.39	9.58	1.38	0.36	1.12	0.07	0.06	0.04

**Figure 2.** Experimental flow chart.

## 2.2. EBSD Analysis

Grain boundary enhancement on IN 617 was done by 15 % cold rolling and annealing at 1100 °C for 1 h. The thermomechanical treatment enhanced the creation of the  $\Sigma 3$  grain boundary selectively. This is a low-energy grain boundary amongst the high-angle grain boundaries: these boundaries improve mechanical properties.  $\Sigma 3$  grain boundaries are also known as twin-grain boundaries. Cold working elongates the grains, and heat treatment makes the new grains grow. The inverse pole figure results from the EBSD analysis are presented in Figure 3. The grain sizes, with and without twins, were calculated by post-processing the data in an OIM analysis electron backscattered diffraction, and their results are tabulated in Table 2. The OIM analysis showed that the grain size of the IN 617 after thermomechanical processing showed a decreasing trend.

**Figure 3.** Inverse pole figure (IPF) map for: (a) IN 617 AR sample; (b) IN 617 GBE sample.

**Table 2.** Microstructural parameters obtained from EBSD for IN 617.

Details	AR IN617	GBE IN617
Average intercept length, $\mu\text{m}$ (including twins $\Sigma 3$ & $\Sigma 9$ )	$28 \pm 4$	$13 \pm 3$
Average intercept length, $\mu\text{m}$ (excluding twins $\Sigma 3$ & $\Sigma 9$ )	$71 \pm 11$	$51 \pm 22$
CSL fraction, %	$62 \pm 1$	$70 \pm 4$
$\Sigma 3$ fraction, %	$61 \pm 1$	$61 \pm 4$

### 2.3. Preparation of Experimental Setup

Air oxidation was performed in a Nabertherm tubular furnace at 700 °C. The samples were placed in thermally stabilised alumina crucibles. The crucibles and sample coupons were weighed individually and together before the start of the experiment. The furnace was allowed to heat up by ramping the temperature up to 700 °C, and then the samples were placed for a long-exposure study of 1000 h. The samples were removed after 100 h, to study weight gain as a function of time.

The steam oxidation test was performed in a custom-built PARR 4650 reactor made of Haynes 230 alloy, as shown in Figure 4. The autoclave was designed for 650 °C/360 bar, 700 °C/ 241 bar and 750 °C/150 bar steam operating conditions. The samples were taken in the form of coupons, and were hung on the hooks of the stirrer. The hooks were made by bending Haynes 556 alloy. The long exposure studies under steam for 1000 h were performed at 700 °C/243 bar for the material coupons in this experiment. The samples were initially weighed before installing them. The temperature was increased by a ramp-and-soak programmed electrical heating mechanism. Excess water was taken initially, and excess volume was vented using needle valves to maintain test pressure. The entire system was protected by using a rupture disk mechanism, which released the pressure immediately, beyond the rated value. The stirring mechanism was operated at 50 rpm, which provided a dynamic simulation of steam, similar to that of power plants: this mechanism was custom-built to suit our application.

**Figure 4.** (a) steam oxidation experimental test facility; (b) sample holder with coupons.

### 2.4. Characterisation

The samples were weighed before and after the oxidation experiment. Weight changes were noted. Initial and final roughness were measured using Bruker 3D Non-contact Profiler Contour GT. At the end of the experiment, surface images and cross-sectional

images were obtained by SEM backscattered and secondary electron modes. On performing energy-dispersive spectroscopy (EDS), using a TSL EDAX liquid-nitrogen-based detector, the composition of the oxide scales formed on the surface and cross-section were obtained. The oxides were re-confirmed by performing powder XRD, and the compositions of the oxides were detected.

### 3. Results

#### 3.1. Comparison of Air and Steam Weight Change

The weight gains at the end of 100 and 1000 h, in the case of air oxidation, and 1000 h, in the case of steam oxidation, are presented in Figure 5. The weight gain increased with increase in exposure time, change in environment from air to steam and increase in grain size. IN 617 AR forms a layer of  $\text{Cr}_2\text{O}_3$  under air oxidation, which is a protective form of oxide, leading to this material faring better in air. The GBE variant fared better than the as-received ones, due to formation of similar protective  $\text{Cr}_2\text{O}_3$  in air with finer grain size. Under steam, both variants of the materials performed well, indicating their superiority at withstanding steam attack at high pressures. The samples performed better in their grain-boundary-enhanced condition: this was due to the thermomechanical treatment proceeding with the reduction in grain size. Grain size played a vital role in corrosion resistance: the finer the grain, the greater the scope for formation of protective chromium oxide. The grain boundary acted as a path for the rapid diffusion of Cr, leading to the formation of  $\text{Cr}_2\text{O}_3$  [14]. A general trend of higher weight gain with increasing exposure times was observed under air oxidation.

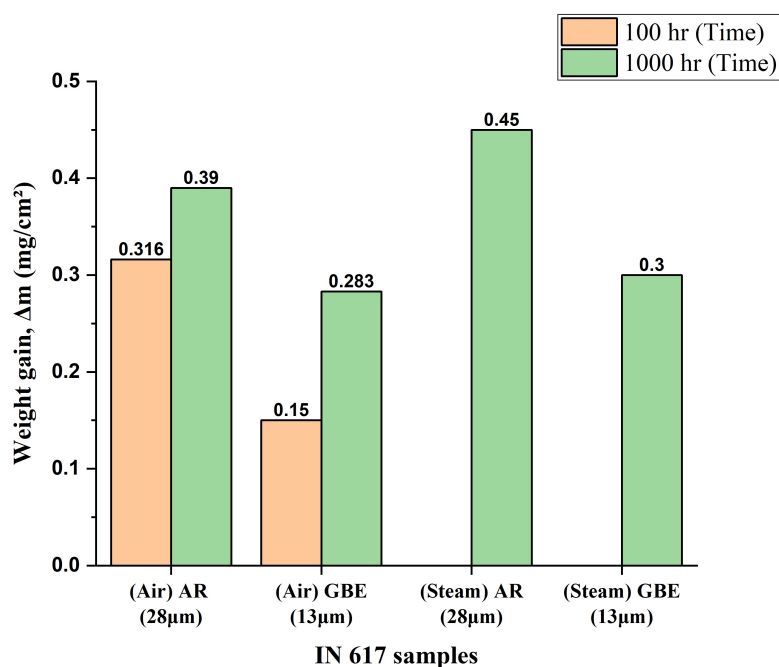


Figure 5. Weight gain of samples with different grain size under air and steam atmospheres.

#### 3.2. Air Oxidation

The surface SEM and EDS elemental mapping for IN 617 AR and IN 617 GBE after 1000 h air oxidation at 700 °C are presented in Figure 6, in which IN 617 AR and IN 617 GBE show major distribution of Cr, Mn, Ti, Ni and O. The oxide covered the entire surface: this was in line with the XRD results, and the presence of multiple phases on the surface facilitated the detection of spinel-based oxides. The precipitates, after long exposure to air oxidation, were titanium carbonitride (black  $\text{Ti}(\text{C},\text{N})$ ) and chromium-rich carbides (grey  $\text{Cr}_{23}\text{C}_6$  and white  $\text{Cr}_6\text{C}$ ) [15]. The roughness values compared post-oxidation are tabulated in Table 3.

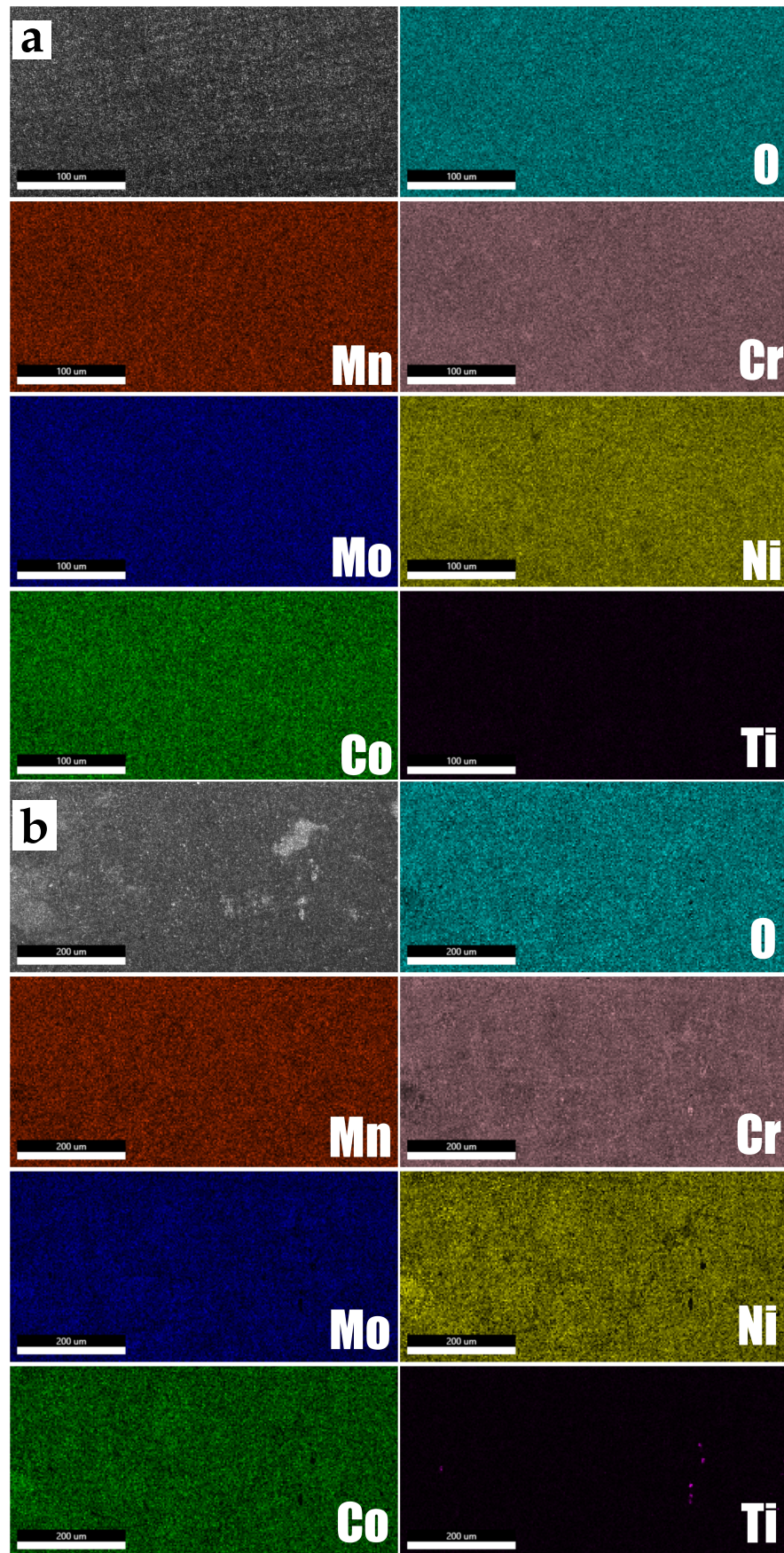


Figure 6. Surface SEM micrograph post-air-oxidation of: (a) IN 617 AR; (b) IN 617 GBE.

**Table 3.** Surface roughness of air-oxidised IN 617 AR and IN 617 GBE sample.

Surface Roughness (Ra)	Initial Condition	Post-Oxidation
IN617 AR	29 nm	139 nm
IN617 GBE	32 nm	142 nm

The cross-section SEM and EDS elemental mapping for IN 617 AR and IN 617 GBE after 1000 h air oxidation at 700 °C are presented in Figure 7. The topmost layer showed oxide scale formation. Cr was selectively enhanced on the top surface, and depleted beneath the layer, indicating external diffusion of Cr. Mo and Co do not form oxides, due to their thermodynamic instability [16]. The alloying elements Mn and Ti are generally incorporated in Cr<sub>2</sub>O<sub>3</sub>. Mn diffuses faster than Ni, Fe and Cr in Cr<sub>2</sub>O<sub>3</sub> scale [17]. The possibility of Mn–Cr spinel was present: hence, a high concentration of Mn was found in the element maps pertaining to cross-section SEM. The presence of O distribution in bulk was detected under air oxidation. The external oxide layer was thin and compact. The oxide scale thickness was measured using ImageJ software (version 1.53t). The topmost oxide covering the substrate, which was compact and defect-free, was measured. This oxide scale on the top prevented further oxidation, while the oxides layers beneath were due to the internal diffusion of the chromium: this did not affect the oxidation in any manner. Hence, only the external oxide layer thickness was accounted for. The diffusion of Cr and Ni leads to formation of Cr<sub>2</sub>O<sub>3</sub> and NiO, which can further combine to form spinel oxides. This inference of probable spinel formation was derived from the literature [18] mentioned in the discussion section: the cross-section SEM results, along with the XRD, substantiated this claim. A similar investigation, carried out by Archana et al. (2021) [7], found a similar trend of oxygen concentration, in cases of air oxidation of IN 617 samples.

### 3.3. Steam Oxidation

The surface SEM and EDS elemental mapping for IN 617 AR and IN 617 GBE after 1000 h steam oxidation at 700 °C/243 bar are presented in Figure 8, in which IN 617 AR and IN 617 GBE show major distribution of Cr, Fe, Ti, Ni and O. The oxide covered the entire surface. This was in line with the XRD results, and the presence of multiple phases on the surface facilitated the detection of spinel-based oxides. The roughness values compared post-oxidation are tabulated in Table 4.

The cross-section SEM and EDS elemental mapping for IN 617 AR and IN 617 GBE, after 1000 h steam oxidation at 700 °C/243 bar, are presented in Figure 9. The topmost layer showed mixed spinel oxide scale formation in the EDS elemental maps. Cr and Fe were selectively enhanced on the top surface, and were depleted beneath the layer, indicating external diffusion of Cr and Fe. The external oxide layer was thin and compact. The oxide scale thickness was measured using ImageJ software. The topmost oxide covering the substrate, which was compact, was measured: this oxide scale on the top prevented further oxidation. The diffusion of Cr and Fe led to formation of Cr<sub>2</sub>O<sub>3</sub>, Fe<sub>3</sub>O<sub>4</sub> and NiCr<sub>2</sub>O<sub>4</sub>. This inference of probable spinel formation was derived from the literature [18] mentioned in the discussion section. The cross-section SEM results, along with the XRD, substantiated this claim.

### 3.4. X-ray Diffraction (XRD) Analysis

Figure 10 displays the XRD analysis performed on the IN 617 AR and IN 617 GBE samples oxidized at 700 °C under air and 700 °C/243 bar steam after 1000 h exposure. The XRD pattern revealed the presence of Cr<sub>2</sub>O<sub>3</sub> and NiCr<sub>2</sub>O<sub>4</sub> for both IN 617 AR and IN 617 GBE under air. IN 617 GBE under steam detected Fe<sub>3</sub>O<sub>4</sub> (magnetite), FeO (wustite), Cr<sub>2</sub>O<sub>3</sub>, FeCo<sub>2</sub>O<sub>4</sub> and NiCr<sub>2</sub>O<sub>4</sub>, while IN 617 AR showed the presence of Fe<sub>3</sub>O<sub>4</sub>, FeCr<sub>2</sub>O<sub>4</sub> and NiCr<sub>2</sub>O<sub>4</sub>. Both the materials, regardless of the oxidizing environment, detected strongly the matrix peaks, indicating that IN 617 AR and IN 617 GBE underwent less severe oxidation.

Rietveld refinement was further performed on the XRD data to evaluate variation in phase percentages, as mentioned in Table 5.

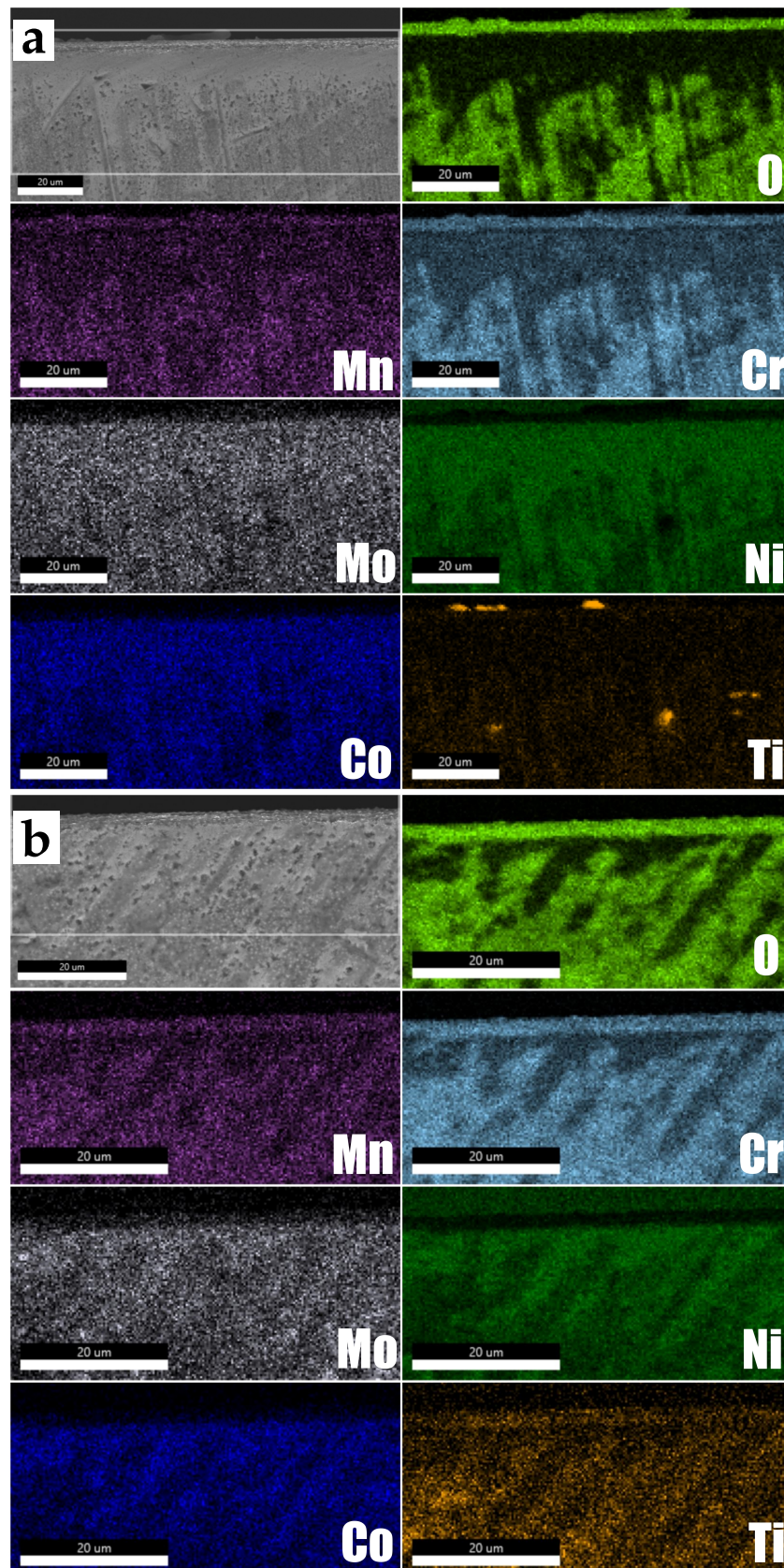


**Figure 7.** Cross-section SEM micrograph post-air-oxidation of: (a) IN 617 AR; (b) IN 617 GBE.

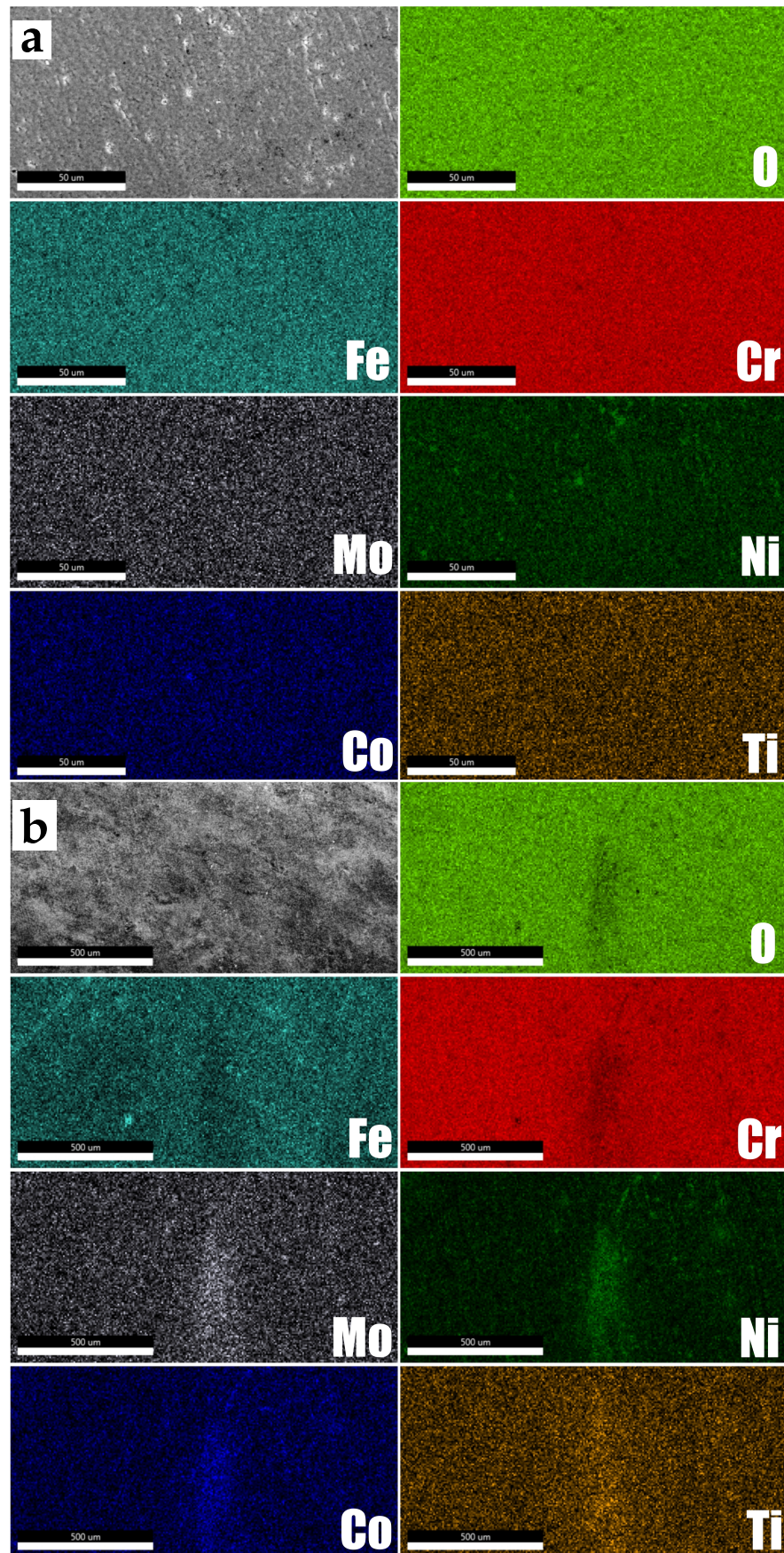
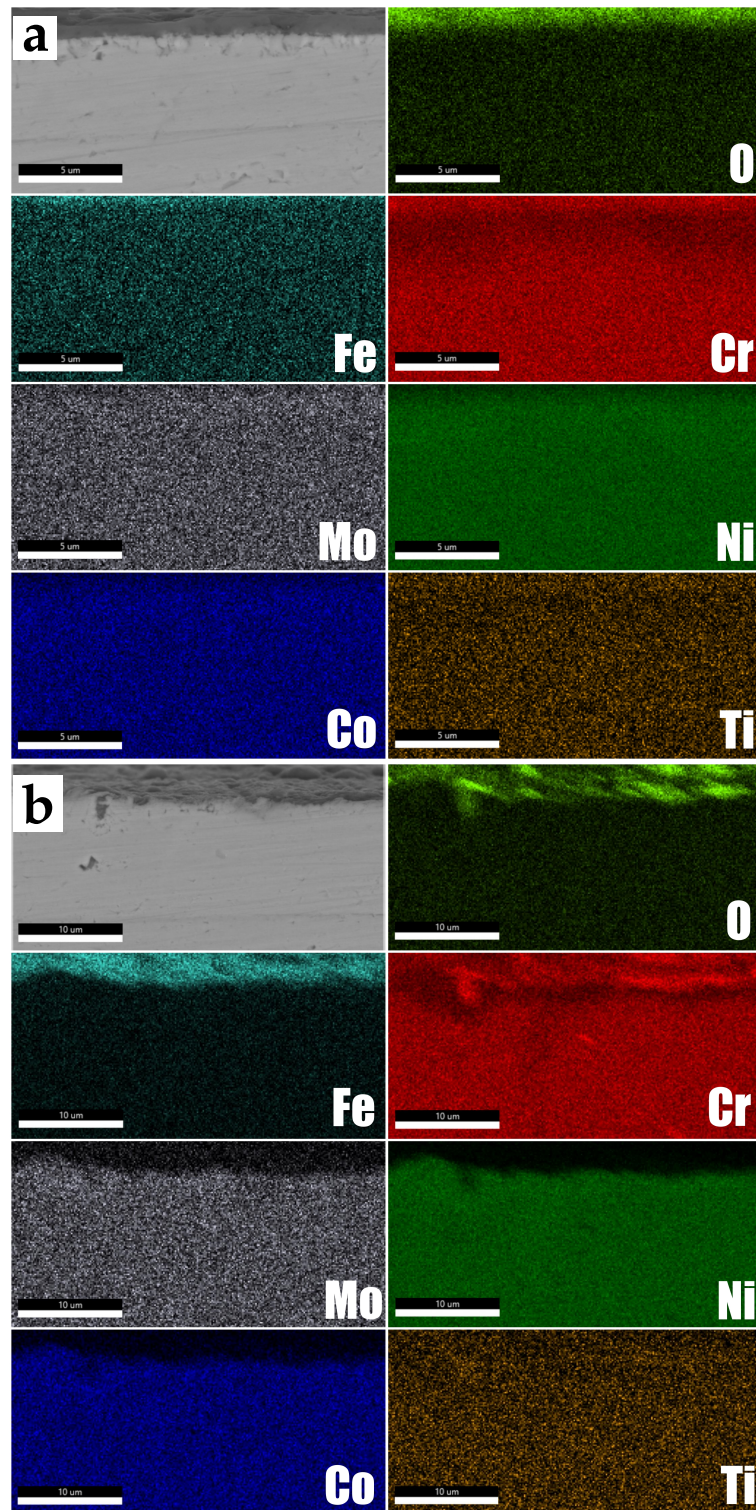


Figure 8. Surface SEM micrograph post-steam-oxidation of: (a) IN 617 AR; (b) IN 617 GBE.

**Table 4.** Surface roughness of steam-oxidised IN 617 AR and IN 617 GBE sample.

Surface Roughness (Ra)	Initial Condition	Post-Oxidation
IN617 AR	29 nm	158 nm
IN617 GBE	32 nm	165 nm

**Figure 9.** Cross-section SEM micrograph post-steam-oxidation of: (a) IN 617 AR; (b) IN 617 GBE.

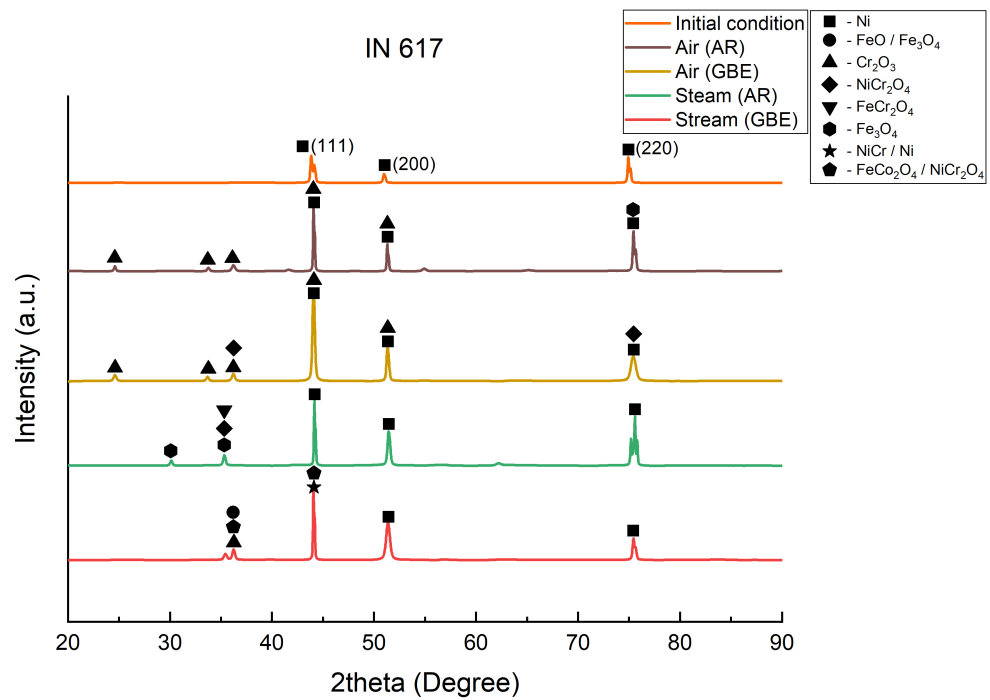


Figure 10. XRD pattern of initial, air-oxidised and steam-oxidised IN 617 alloy.

Table 5. Oxides detected in XRD under Rietveld analysis post-oxidation.

Material and Condition	Major Elements Detected	Remaining
IN 617 AR (under air)	Cr <sub>2</sub> O <sub>3</sub> —26.8% NiCr <sub>2</sub> O <sub>4</sub> —6%	Ni
IN 617 GBE (under air)	Cr <sub>2</sub> O <sub>3</sub> —27.1% NiCr <sub>2</sub> O <sub>4</sub> —21%	Ni and Cr
IN 617 AR (under steam)	Fe <sub>3</sub> O <sub>4</sub> —1.2% FeCr <sub>2</sub> O <sub>4</sub> —17.8% NiCr <sub>2</sub> O <sub>4</sub> —10.8%	Ni
IN 617 GBE (under steam)	Fe <sub>3</sub> O <sub>4</sub> —6.6% Cr <sub>2</sub> O <sub>3</sub> —1.8% FeCo <sub>2</sub> O <sub>4</sub> —7.5% FeO—6.3% NiCr <sub>2</sub> O <sub>4</sub> —8.3%	Ni and Cr

#### 4. Discussion

The mechanism for the growth of the duplex layer in cases of Ni-Fe-Cr alloys is by mixed-growth model, as shown in Figure 11. The oxides of Ni and Cr are formed in the form of NiO and Cr<sub>2</sub>O<sub>3</sub> (chromia): the reasons for the formation of these oxides is that the element has Ni majorly, and Cr diffuses fastest amongst the present element (Fe < Ni < Cr). With increase in exposure time, the nickel-based oxides increase, relative to the chromia: in order to maintain the stability of the oxides, they recombine to form spinel-based oxide, like NiCr<sub>2</sub>O<sub>4</sub> (nichromite). The spinel-based oxides are porous in nature and, hence, Fe and Ni diffuse outwards selectively, and form a further layer of spinel oxides, like FeCr<sub>2</sub>O<sub>4</sub> (trevorite). The porous trevorite further allows the internal diffusion of oxygen, which combines with chromium to form chromia: this acts as a protective scale, over which the spinel oxides exist. Chromium diffuses more slowly than iron and nickel when the latter exist in spinel form: specifically, for Fe-rich alloys like 800H, Fe<sub>3</sub>O<sub>4</sub> is formed instead of NiO near the surface [18].

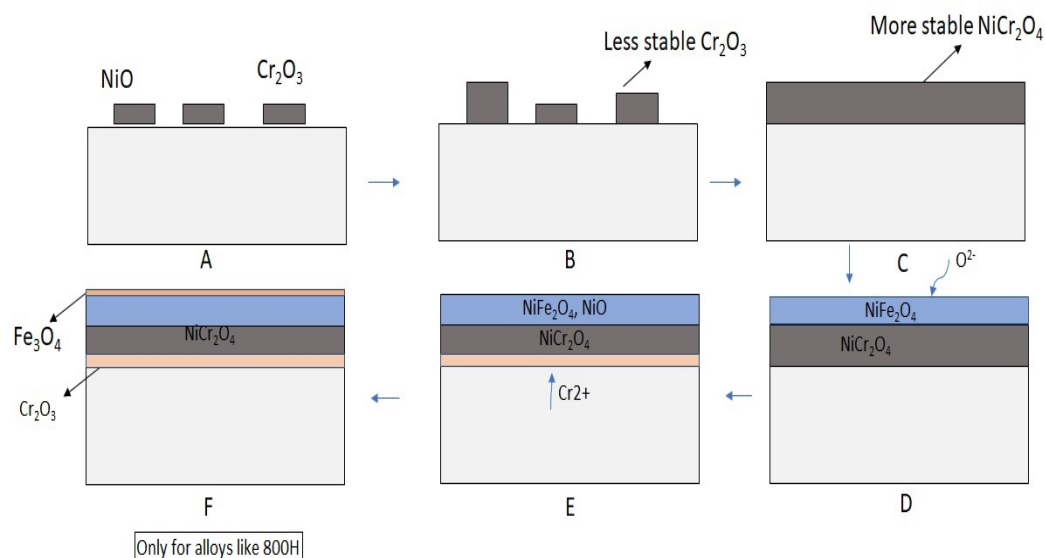


Figure 11. Oxide growth mechanism of IN 617 alloy.

## 5. Conclusions

- IN 617 GBE outperformed IN 617 AR, owing to thermomechanical process optimization, which resulted in smaller grain size.
- The weight gain increased with increase in exposure time, change in environment from air to steam and increase in grain size.
- IN 617 under air and steam formed protective Cr-based oxides.
- The severity of oxidation for IN 617 was less overall, and the XRD results showed matrix phases, even after oxidation.
- This material satisfactorily resisted steam corrosion under high-temperature and high-pressure conditions.

**Author Contributions:** Conceptualisation, R.K., S.S., V.S.S. and M.K.; methodology, R.K. and S.S.; software, R.K. and V.S.S.; validation, R.K.; investigation, R.K.; resources, S.S., V.S.S. and M.K.; data curation, R.K.; writing—original draft preparation, R.K.; writing—review and editing, S.S., V.S.S. and M.K.; visualisation, R.K.; supervision, S.S., V.S.S. and M.K.; project administration, S.S.; funding acquisition, S.S., V.S.S. and M.K. All authors have read and agreed to the published version of the manuscript.

**Funding:** This research was funded by ARCI, sanction No. ARC/FIN/SNCD/2018/IITM/A1.

**Institutional Review Board Statement:** Not applicable.

**Informed Consent Statement:** Not applicable.

**Data Availability Statement:** Data sharing not applicable.

**Acknowledgments:** The authors would like to thank their EnERG labmates and their texture and microstructure labmates for their support.

**Conflicts of Interest:** The authors declare no conflict of interest.

## References

1. Khatib, H. IEA world energy outlook 2011—A comment. *Energy Policy* **2012**, *48*, 737–743. [CrossRef]
2. Evans, S.; Pearce, R. Mapped: The World's Coal Power Plants. *Carbon Brief*. Available online: <https://www.carbonbrief.org/mapped-worlds-coal-power-plants/> (accessed on 28 September 2022).
3. Zhang, T. Methods of improving the efficiency of thermal power plants. *J. Phys. Conf. Ser.* **2020**, *1449*, 012001. [CrossRef]

4. Ghosh, N.; D'souza, R. Why 2070 Is Justified as the Net-Zero Deadline Year for India. Available online: <https://policycommons.net/artifacts/1900130/why-2070-is-justified-as-the-net-zero-deadline-year-for-india/2651297/> (accessed on 28 September 2022).
5. Zhang, D. Introduction to advanced and ultra-supercritical fossil fuel power plants. In *Ultra-Supercritical Coal Power Plants*; Elsevier: Amsterdam, The Netherlands, 2013; pp. 1–20.
6. Nandi, S.; Jaipal Reddy, G.; Singh, K. Effect of Ageing on Creep behaviour of IN 617 Nickel Base Super Alloy for Advanced USC Power Plant Applications. *Trans. Indian Inst. Met.* **2016**, *69*, 271–276. [[CrossRef](#)]
7. Archana, M.; Rao, C.; Ningshen, S.; Philip, J. High-temperature air and steam oxidation and oxide layer characteristics of alloy 617. *J. Mater. Eng. Perform.* **2021**, *30*, 931–943. [[CrossRef](#)]
8. Hari, P.; Arivazhagan, N.; Rao, M.N.; Pavan, A. Oxidation studies on nickel-base superalloy 617 OCC. *Mater. Today Proc.* **2020**, *27*, 2763–2767. [[CrossRef](#)]
9. Staszewska, K.; Scendo, M. Mechanism and kinetics oxidation of Inconel 617 and 625 alloys. *Tech. Issues* **2016**, *1*, 82–89.
10. Holcomb, G.R. High pressure steam oxidation of alloys for advanced ultra-supercritical conditions. *Oxid. Met.* **2014**, *82*, 271–295. [[CrossRef](#)]
11. Yang, J.; Wang, S.; Xu, D. High temperature oxidation of alloy 617, 740, HR6W and Sanicro 25 in supercritical water at 650 °C. *Corros. Eng. Sci. Technol.* **2020**, *55*, 196–204. [[CrossRef](#)]
12. Katnagallu, S.S.; Mandal, S.; Cheekur Nagaraja, A.; De Boer, B.; Vadlamani, S.S. Role of carbide precipitates and process parameters on achieving grain boundary engineered microstructure in a Ni-based superalloy. *Metall. Mater. Trans. A* **2015**, *46*, 4740–4754. [[CrossRef](#)]
13. Basak, S.; Sharma, S.K.; Sahu, K.K.; Gollapudi, S.; Majumdar, J.D. Surface modification of structural material for nuclear applications by electron beam melting: Enhancement of microstructural and corrosion properties of Inconel 617. *SN Appl. Sci.* **2019**, *1*, 1–12. [[CrossRef](#)]
14. Kim, J.H.; Kim, D.I.; Suwas, S.; Fleury, E.; Yi, K.W. Grain-size effects on the high-temperature oxidation of modified 304 austenitic stainless steel. *Oxid. Met.* **2013**, *79*, 239–247. [[CrossRef](#)]
15. Mehdizadeh, M.; Farhangi, H. Precipitation behavior and mechanical properties of IN 617 superalloy during operating at 850° C. *Int. J. Press. Vessel. Pip.* **2022**, *198*, 104674. [[CrossRef](#)]
16. Christ, H.J.; Künecke, U.; Meyer, K.; Sockel, H. Mechanisms of high-temperature corrosion in helium containing small amounts of impurities. II. Corrosion of the nickel-base alloy Inconel 617. *Oxid. Met.* **1988**, *30*, 27–51. [[CrossRef](#)]
17. Al-Hatab, K.A.; Al-Bukhaiti, M.; Krupp, U. Cyclic oxidation kinetics and oxide scale morphologies developed on alloy 617. *Appl. Surf. Sci.* **2014**, *318*, 275–279. [[CrossRef](#)]
18. Ghule, B.; Sundaresan, C.; Vijayshankar, D.; Raja, V. Oxidation Behaviour of Ni-Base Superalloys in Supercritical Water: A Review. *J. Indian Inst. Sci.* **2022**, *102*, 351–389. [[CrossRef](#)]

**Disclaimer/Publisher's Note:** The statements, opinions and data contained in all publications are solely those of the individual author(s) and contributor(s) and not of MDPI and/or the editor(s). MDPI and/or the editor(s) disclaim responsibility for any injury to people or property resulting from any ideas, methods, instructions or products referred to in the content.